

Jet termination in wide-angle tailed radio sources

M.J. Hardcastle¹ and I. Sakelliou²

¹ *Department of Physics, University of Bristol, Tyndall Avenue, Bristol BS8 1TL*

² *School of Physics and Astronomy, University of Birmingham, Edgbaston, Birmingham B15 2TT*

10 October 2018

ABSTRACT

Wide-angle tail radio galaxies (WATs) are an uncommon class of radio sources with luminosities near the FRI/FRII break, and are usually associated with central cluster galaxies. Their defining characteristic when imaged sensitively at high resolution is their twin, well-collimated jets, which can persist with low opening angle for tens of kpc before flaring into long, often bent plumes. Although several models for the jet termination have been proposed, the majority of them are unsatisfactory when confronted with observations. Here we present the results of a programme of radio observations made with the aims of showing that objects classified as WATs do all have well-collimated jets and seeing in detail *how* the jets disrupt as they enter the plumes. We show that compact, ‘hotspot-like’ features at the ends of the jets are common but by no means universal, and discuss the constraints that this places on models of the jet-plume transition. We discuss the properties of the observed well-collimated jets and, using relativistic beaming models, estimate their speed to be $\sim 0.3c$. Finally, we show that the distance from the galactic centre at which the base of the plume is found is related to the temperature of the host cluster.

Key words: galaxies: active – galaxies: jets

1 INTRODUCTION

The term ‘wide-angle tail radio galaxy’ (WAT) is used in the literature in a number of different ways. In this paper we use it (following Leahy 1993) to refer to a clearly identified population of radio galaxies, which are always associated with a cluster dominant galaxy, at or near the cluster centre, and are characterized in the radio by twin, well-collimated jets which may continue for tens of kpc before abruptly flaring into long, often sharply bent plumes or tails. The bending of the plumes, the feature which originally gave the class its name, has long been a source of interest (e.g. Eilek et al. 1984); a plausible explanation is ram pressure from large-scale bulk motions in the host cluster due to cluster-cluster mergers (Loken et al. 1995) and this is supported by the facts that the host clusters of bent sources often show an X-ray structure which is elongated in the same direction as the WAT tails (Gómez et al. 1997) and that bent sources are often displaced from the X-ray centroids of their host clusters (Sakelliou & Merrifield 2000). In this paper we concentrate on the termination of the well-collimated jets. We regard this as a separate problem from that of the large-scale plume bending, both because of the existence of relatively straight objects that are WATs by our definition (e.g. 3C 130, Hardcastle 1998) and because there are well-known cluster-centre objects that do not contain WAT-type jets but show very similar large-scale bending (e.g. 3C 75, Eilek & Owen 2002; Appendix A).

The termination of the WAT jets is an outstanding problem with our present understanding of how radio sources interact with the intracluster medium. In the (few) well-studied objects the jets resemble those in classical double (FRII) radio sources, in which the jet termination is due to a strong shock as jet plasma interacts with the external medium, giving rise to a hotspot. But in WATs, which have luminosities similar to those of FRIIs, the jets terminate not at the very ends of the sources, but near the base of the plumes. The outstanding question is therefore: what causes the jets to disrupt? This is also a key question if we wish to test models that try to explain the bending and distortion of the plumes: it is the physical processes that take place at the jet termination that define the plumes’ nature and characteristics.

Because WATs are rare compared to other classes of radio galaxies, there have been few detailed radio observations which might help to explain why WAT jets disrupt. Radio observations of samples of WATs (e.g. O’Donoghue, Owen & Eilek 1990) have concentrated on their large-scale structure and the dynamics of plume bending. Images of this kind usually show a well-collimated inner jet, and typically show a bright ‘flare point’ at the base of the plume, sometimes referred to (e.g. O’Donoghue, Eilek & Owen 1993) as a hotspot, but do not have enough resolution to resolve it transversely and give structural information on the jet termination; thus, in general, we cannot say *how* the jets disrupt. However, Hardcastle (1998) showed that the WAT 3C 130 ($z = 0.109$) exhibits a bright, compact, sub-kpc feature

at the termination of the N jet. The similarity of this feature to the terminal hotspots in FRIIs led Hardcastle (1998) to suggest that 3C 130's N jet also terminated in a shock; further multi-frequency observations suggest that the absence of a comparable feature in the S plume is reflected in the source's particle acceleration properties (Hardcastle 1999). These observations motivated us to carry out a comparably detailed study of a larger sample of WATs, with the aim of determining the properties of the inner jets and the nature of the jet termination in the WAT population as a whole. In this paper we present the new radio observations and discuss some conclusions that can be drawn from them.

Throughout the paper we use a cosmology with $H_0 = 65 \text{ km s}^{-1} \text{ Mpc}^{-1}$, $\Omega_m = 0.3$ and $\Omega_\Lambda = 0.7$. Spectral indices α are defined in the sense $S \propto \nu^{-\alpha}$. B1950.0 co-ordinates are used.

2 SAMPLE, OBSERVATIONS AND ANALYSIS

The sample we chose to observe in the radio was a subset of the sample of Sakelliou & Merrifield (2000), who based their object list on the radio survey of Abell clusters by Owen & Ledlow (1997, and references therein). From that sample we chose a few objects that were approximately at the centres of their host clusters and that clearly showed the flaring at the base of the plumes that characterizes the class, although not all of them were known to have faint, narrow inner jets. There was otherwise no morphological selection. To supplement this sample we added one southern source, 1610–608, which was not in Owen & Ledlow's survey because of its declination but which otherwise met our selection criteria. The properties of the observed sample are listed in Table 1. We emphasise that this is in no sense a statistically complete sample, and that it is possible that our morphological selection, based on low-resolution maps, has introduced some bias that renders these objects unrepresentative of the parent population of WATs as we define them. However, we hope that the structures we observe in jet terminations in the sample should be representative of those of the WAT population as a whole. As we will discuss later (Section 4.1) our observations give us reason to believe that WATs (according to our definition) can indeed be safely identified from low-resolution radio maps.

We chose to observe the northern sources in our sample using the NRAO Very Large Array (VLA) at 8.5 GHz. This observing frequency was chosen because of the high angular resolution it allows (up to ~ 0.25 arcsec in the A configuration of the VLA) and because the use of high frequencies mitigates the potentially important effects on the sources' polarization properties of Faraday rotation due to the intra-cluster medium (discussed further below).

Since the main aim of our observations was high angular resolution, the majority of the newly allocated observing time was spent in the A- and B-configurations of the VLA, with only short observations at C- and D-configurations. All our new VLA observations used two observing frequencies at 8.44 and 8.49 GHz, with a bandwidth of 25 MHz (for the A-configuration observations, to avoid bandwidth smearing) and 50 MHz (for the rest). However, we obtained C- and D-configuration data for half of our sources from the VLA archive, making use of long existing observations at similar frequencies taken for other purposes and published elsewhere (Katz-Stone et al. 1999; Eilek &

Table 3. ATCA observations of 1610–608

Configuration	Date	Duration (hours)
6A	2000 Oct 07	9.6
1.5E	2000 Nov 24	7.8

Owen 2002). Details of the VLA observations used are given in Table 2. The initial data reduction was carried out in AIPS in the standard manner. Individual datasets were phase self-calibrated to convergence, where enough CLEAN components were available. In 3C 465 and 1433+553 there was some evidence of core variability over the epochs of observation, and so the task UVSUB was used to bring the core flux densities into agreement. The datasets were then cross-calibrated and merged, beginning with the highest-resolution data (so that B-configuration data were cross-calibrated with A-configuration data and merged, C-configuration data cross-calibrated with the resulting A+B dataset and merged, and so on) to give a final dataset containing phase-aligned A,B,C and D-configuration data. We weighted down the short-baseline datasets in the cases with long C- and D-configuration observations in order to avoid being dominated by these data in the imaging stages; otherwise reweighting on merging reflected only the bandwidth of the observations.

The southern source 1610–608 was observed with the ATCA in two configurations, as shown in Table 3, at 4.80 and 8.64 GHz. The initial data reduction for this source was carried out in MIRIAD, and again followed standard procedures. The data were then self-calibrated, cross-calibrated, and merged in AIPS. Strong RFI during the second observing run necessitated significant data flagging, so the overall u, v coverage is not as good as might be expected.

The final imaging was carried out in AIPS using the task IMAGR, combining the two observing frequencies (in the case of the VLA data) or the 13 spectral channels (in the case of the ATCA data) to make single images, which for the VLA data are at an intermediate effective frequency of 8.47 GHz. The u, v plane was weighted (using the ROBUST and UVTAPER parameters of IMAGR) to obtain the desired resolution. Images, in all cases based on the full combined datasets, are presented in the following section.

3 IMAGES

In this section we present total-intensity and polarization images of each of the sources in our sample. In most cases, a low-resolution image is presented to show the large-scale structure of the source; high-resolution images of the jet terminations can then be seen in context. Properties of the maps presented are given in Table 4. We comment briefly on each source in turn.

A note of caution is necessary regarding polarization maps. At our observing frequency, Faraday rotation is negligible (involving corrections to the polarization position angle of $\lesssim 5^\circ$) if the magnitude of the rotation measure (RM) towards a particular point on the source is $\lesssim 70 \text{ rad m}^{-2}$. If Faraday rotation is negligible, then the direction of the B -field in the incoming radio waves, which is the direction of the vectors we plot in all the polarization maps that follow, tells us the (emission-weighted mean) magnetic field direction in the synchrotron-emitting plasma. However, all our sources lie in cluster environments, and several of them are in rich clusters for which RM magnitudes higher than 70 rad m^{-2} are frequently observed.

Table 1. The observed sample

Source name	Other name	Abell cluster	z	Angular scale (kpc arcsec $^{-1}$)	1.4-GHz flux density (Jy)	$\alpha_{1.4}$	1.4-GHz luminosity (W Hz $^{-1}$ sr $^{-1}$)
0647+693	4C 69.08	562	0.11	2.16	0.800	1.03	2.3×10^{24}
1231+674	4C 67.21	1559	0.1049	2.07	0.879	0.88	2.3×10^{24}
1333+412	4C 41.26	1763	0.2278	3.93	0.797	1.08	1.2×10^{25}
1433+553	4C 55.29	1940	0.1402	2.66	0.447	0.79	2.1×10^{24}
2236–176	PKS	2462	0.0742	1.52	1.642	0.78	2.0×10^{24}
3C 465		2634	0.0302	0.65	7.650	0.82	1.5×10^{24}
1610–608	PKS	3627	0.0157	0.34	48	1.24	2.5×10^{24}

Redshifts are taken from Owen, Ledlow & Keel (1995), except for that of 0647+693 (Stickel & Kühr 1994) and 1610–608 (the cluster redshift, corrected for Local Group motions, from Struble & Rood 1999). 1.4-GHz flux densities are from Ledlow & Owen (1995), except for 1610–608, where the flux density is from Christiansen et al. (1977). Spectral indices, are determined from lower-frequency observations where possible: 6C 151-MHz flux densities for 0647+693, 1231+674, 1333+412 and 1433+553, the MRC 408-MHz flux density for 2236–176, the 3CRR 178-MHz flux density for 3C 465, and the 843-GHz MOST observations of Jones & McAdam (1992) for 1610–608. These spectral indices are used to calculate the 1.4-GHz luminosity in the source frame.

Table 2. Observations made with the VLA

Source	A configuration		B configuration		C configuration		D configuration	
	Date	Time (h)	Date	Time (h)	Date	Time (h)	Date	Time (h)
0647+693	2001 Jan 15	2.0	2001 May 19	1.5	2001 Jul 19, 29	1.0	2001 Dec 19, 20	0.5
1231+674	2001 Jan 15	2.0	2001 May 19	1.5	1992 Apr 30 ^a	3.0	1992 Aug 6, 11, 18 ^a	4.6
1333+412	2001 Jan 16	2.0	2001 May 19	1.5	2001 Jul 29	1.0	2001 Dec 20	0.5
1433+553	2001 Jan 16	2.0	2001 May 19	1.5	1992 Apr 30 ^a	3.0	1992 Aug 6, 11, 18 ^a	4.3
2236–176	2001 Jan 15	2.0	2001 May 19	1.5	2001 Jul 19	1.0	2001 Dec 19	0.5
3C 465	2001 Jan 15	2.0	2001 May 19	1.5	1989 Sep 20 ^b	6.7	1989 Dec 01 ^b	1.3

Notes: ^a Observations made by D.M. Katz-Stone at an observing frequency of 8.41 GHz. ^b Observations made by J.A. Eilek at observing frequencies of 8.0 and 8.5 GHz. All observations, except for those at A-array, used two channels with a bandwidth of 50 MHz.

The only direct observational evidence we have on individual sources (except for 1610–608, which we discuss in more detail below) comes from the observations of 3C 465 by Eilek & Owen (2002), which show the magnitude of RM to range up to ~ 250 rad m $^{-2}$ in small, discrete regions: this would imply polarization corrections of around 20°. However, 3C 465’s host cluster may not be representative. It should therefore be borne in mind that the polarization vectors we plot are only the best estimate available of the true B -field directions, although for simplicity we describe them as magnetic field vectors in what follows.

The reader is reminded that we use the term ‘jets’ only for the inner, well-collimated structures in the WATs. The brighter, broader features which dominate the sources’ radio emission are referred to as ‘plumes’. The central unresolved feature, coincident with the nucleus of the host galaxy, is the ‘core’ and we tabulate core properties, measured from high-resolution maps, in Table 5.

3.1 0647+693

No detailed radio observations of this source had previously been made. Based on a snapshot image, O’Dea & Owen (1985) remarked that the source’s structure is intermediate between narrow-angle and wide-angle tails, an impression reinforced by our data. Gómez et al. (1997) showed that the radio source is significantly (30 arcsec) to the west of the cluster X-ray peak. DSS2 images show that the host galaxy is also 21 arcsec to the west of a second bright elliptical, although the host does appear to be the brighter of the two by around 0.5 mag in R .

Our low-resolution maps (Fig. 1) show that the plumes,

Table 5. Properties of the radio cores of the sample

Source	Core flux density (mJy)	RA (B1950)	DEC (B1950)
0647+693	4.9	06 47 54.72	+69 23 31.2
1231+674	5.5	12 31 02.58	+67 24 15.6
1333+412	3.3	13 33 09.64	+41 15 22.6
1433+553	15.1*	14 33 54.83	+55 20 54.2
2236–176	11.8	22 36 30.22	–17 36 06.8
3C 465	214*	23 26 00.44	26 45 21.26
1610–608	130	16 10 43.08	–60 46 54.2

Core fluxes quoted are the integrated values from Gaussian fitting to high-resolution maps using the AIPS task JMFIT; the positions quoted are also JMFIT output. Flux densities marked with an asterisk indicate that the core had detected variability between the epochs of our observations.

particularly the southern plume, are not abnormal for a WAT. However, the high-resolution maps (Fig. 2) show that the inner jets are very much more bent than in any of the other objects in our sample; the southern jet is detected over almost all its length, and (in projection) makes two sharp, almost 90° bends at the positions labelled SJ1 and SJ2 in Fig. 2. The northern jet is less well detected but appears to have bent in a similar way by the time it becomes visible at NJ1. If the jet is ballistic in this source (cf. Blandford & Icke 1978), the strong bending would require the source to have been moving eastwards on average almost as fast as the jet flow (and faster at some times) which seems unlikely (we discuss jet speeds in more detail below, section 4.2). Instead, it is tempting to attribute both the jet bending and the general direction of the plumes to ram pressure as a result of

Table 4. Properties of the maps presented

Source	Restoring beam			Off-source noise		Figure number
	Major axis (arcsec)	Minor axis (arcsec)	Pos. angle (degree)	Stokes <i>I</i> (μ Jy)	Stokes <i>Q, U</i> (μ Jy)	
0647+693	2.03	1.84	73	24	25	1
	0.90	0.61	59	23		2
1231+674	2.38	1.98	-62	11	11	3
	1.24	0.73	-58	12	12	4
1333+412	1.28	0.81	-65	15	15	5
	0.38	0.27	-76	13		6
1433+553	2.32	1.81	-59	12	12	7
	1.04	0.55	-65	12	13	8
2236-176	2.59	1.82	10	18	15	9
	0.78	0.52	23	13	15	10
3C 465	2.60	2.03	-68	26	12	11
	0.61	0.60	53	26	20	12
1610-608	2.52	1.78	-10	740	300	13
	1.30	1.01	3	430	78	13

bulk motion of the host galaxy towards the cluster centre and/or the neighbouring elliptical.

The N jet cannot be reliably traced into the N plume, but it seems most likely that it terminates in the compact (arcsec-scale, comparable in size to the jet) feature N1 at the N edge of the N plume. In the S plume it is not clear whether the jet terminates in S1 or S2, but S2 contains the most convincing compact structure.

3.2 1231+674

This source has previously been imaged by O’Donoghue et al. (1990) and Katz-Stone et al. (1999). The image of the large-scale structure (Fig. 3) thus shows few new details. The arc appearing perpendicular to the S plume, commented on by O’Donoghue et al., turns out to have an unresolved radio core identified with an optical galaxy in the field visible in the DSS2 plates. It is thus most likely to be a narrow-angle tail (NAT) radio galaxy falling into the potential well of A1559. The host galaxy of 1231+674 itself is a dumb-bell system aligned approximately E-W on the sky, with the radio source being associated with the brighter western component.

The high-resolution image (Fig. 4) shows two well-defined jets. The N jet bends smoothly and terminates in the bright region N1; this region contains some compact structure, elongated in the jet direction, whose magnetic field direction is transverse to the jet direction. The S jet bends abruptly at two knots, S1 and S2, in which the magnetic field is transverse to the jet direction, but then there appears to be continued well-collimated outflow, with a longitudinal magnetic field, from S2 to the eventual jet termination in the diffuse region S3. 1231+674, like 3C 130, is a source in which the jet termination is not associated with significant observed bending in the plumes.

3.3 1333+412

This small source has not been observed previously at high resolution; the best previous maps are those of Owen & Ledlow (1997). Our low-resolution image (Fig. 5) shows much the same features, but gives a clear detection of the inner jets. The small source to the E is associated with one of the many fainter

galaxies in the field, and is likely to be a NAT lying in the cluster. The N lobe is noticeably less strongly polarized than the S lobe. Since the cluster environment of 1333+412 is known to be rich, this is plausibly due to depolarization from the intra-cluster medium (ICM).

The high-resolution image (Fig. 6) shows the S jet penetrating into the plume for some distance (SJ1) before it terminates in the compact region S1. The current termination position of the N jet is not clear; it points towards either N2 or N3, but the brightest feature in the plume is N1.

3.4 1433+553

This source was previously observed by O’Donoghue et al. (1990) and Katz-Stone et al. (1999). The image of the large-scale structure (Fig. 7) is similar to others previously presented. The S lobe is unusual in that it shows no obvious evidence, either in total intensity or polarization, for a plume leading away from the source. It is possible that the plume makes a small angle to the line of sight, so that we are seeing it in projection.

The high-resolution image (Fig. 8) shows the S jet bending (SJ1) before it enters a reasonably compact bright region, S1. The N jet is not traced all the way into the N plume at this resolution, but there is a clear compact feature (N1) in the plume with an unusual ‘shock-like’ structure.

3.5 2236-176

This source was previously observed by O’Donoghue et al. (1990), and our low-resolution image (Fig. 9) shows similar features; the noteworthy feature of the source is the 90° bend in the E plume. On smaller scales, our high-resolution image (Fig. 10) shows a well-collimated, asymmetrical pair of jets (NJ1, SJ1) which bend with S-symmetry at about the same distance from the nucleus (NJ2, SJ2). The fainter N jet appears to retain its collimation (NJ3) until it disappears into a diffuse region of high-surface-brightness emission (N1) with no obvious compact features at the base of the plume. The S jet is similar, although there is a faint compact feature (S1) which may be associated with the jet termination.

3.6 3C 465

3C 465 has been imaged in several earlier studies, including Leahy (1984), Eilek et al. (1984) and, most recently, Eilek & Owen (2002). Its large-scale properties (Fig. 11) are well known.

At high resolutions (Fig. 12), knotty structure in its one-sided jet is visible (NJ1) but there is no compact structure after the jet bends W at NJ2, although a distinct region downstream (N1) is visible in total intensity and polarization. The high-surface-brightness base of the S plume is well resolved, showing filamentary structures (S1, S2) that are not obviously related to the termination of the S jet.

3.7 1610–608

1610–608 lies in the nearby massive cluster Abell 3627 (Böhringer et al. 1996) which has been suggested as the core of the so-called ‘Great Attractor’ (e.g. Kraan-Korteweg et al. 1996). The radio source was shown to have WAT-like structure by the low-resolution ATCA observations of Jones & McAdam (1996); its proximity gives it a claim to be called the closest WAT source. Ours are the first high-resolution observations. Because we do not have short-baseline data, the large-scale structure of the source is not shown. However, our observations (Fig. 13) clearly show the characteristic inner jets of the WAT class. Neither jet appears to terminate in any particularly compact structure. The inner regions of the source are quite strongly polarized, and there is little evidence for depolarization between the two frequencies, but the position angles of the polarization vectors differ markedly between 5 and 8 GHz, particularly in the E plume, suggesting that a resolved Faraday screen is present.

4 RADIO PROPERTIES OF WIDE-ANGLE TAILS

4.1 WAT morphology

All the sources in our sample clearly show the narrow, well-collimated inner jets, leading from the nucleus to the broader plumes, that we regard as a defining characteristic of the class; in some cases (0647+693, 1333+412, 1610–608) the jets are detected for the first time by our observations. This illustrates that WATs can reliably be identified from low-resolution images on the basis of their ‘flaring’ morphology. We find that many of the jet-plume transitions are not associated with significant plume bending; in fact, if we exclude 0649+693, 9/12 of the plumes in the present sample do not apparently bend strongly at or near the transition. It seems unlikely that such a large number of relatively straight jet-plume transitions could be explained by fortuitous projection effects.

The main surprise from the point of view of source structure was the inner jets in 0647+693, with their clear large-scale bending. We suspect that there has been a bias against such objects in previous high-resolution radio imaging work, since a number of candidate objects with similar plume behaviour can be identified in the images of Owen & Ledlow (1997); we hope to investigate their inner jet properties with future VLA observations. The existence of the hotspot, and the well-collimated jets in this source, provide an additional argument against models that invoke ram pressure to explain the jet termination or jet disruption; these jets appear to be bending due to ram pressure well before their termination, which would not be expected in

the models of Loken et al. (1995). This, together with the observation that plumes are often initially straight, reinforces earlier arguments (Section 1) that the plume bending and jet termination in WATs are separate and unrelated problems.

It is worth noting that the magnetic field direction in the jets is generally parallel to the jet direction, as we might expect for FR II-like jets. In more normal FR I jets, there is typically a transition from a parallel to a perpendicular field configuration, which usually occurs on scales of a few kpc (see Appendix A for an example).

4.2 Speeds and beaming

Our good images of the jets allow us to determine jet/counterjet ratios (jet sidednesses) for the sample. These are listed in Table 6; we follow the procedure defined by Hardcastle et al. (1998) and measure only the straight part of the jet, to ensure that there is no change in the angle it makes with the line of sight over the integration region. As O’Donoghue et al. (1993) remarked (with a sample containing several sources in common with ours) the jet sidednesses are generally close to unity. If we assume that the jets are intrinsically symmetrical and that the jet sidedness ratio is due to relativistic beaming effects, we can constrain the characteristic beaming speed β . There is no direct independent evidence for relativistic speeds in these jets, although it is interesting that the two sources that show variable radio cores (an indication of beaming) also show comparatively one-sided jets. Nevertheless, it seems plausible that beaming accounts for a substantial fraction of the jet-counterjet asymmetry. The maximum-likelihood value of β , for the jets (if we assume that they sample all possible angles to the line of sight and that the jets are intrinsically symmetrical) is around 0.3; this is also true for the O’Donoghue et al. objects and for the combination of the two samples, for which we find $\beta = 0.3 \pm 0.1$, determining errors using a Monte Carlo technique. These WAT characteristic speeds are thus significantly lower than those measured by Wardle & Aaron (1997) for FR II quasars, or Hardcastle et al. (1999) for FR II radio galaxies, but it is not clear that the WAT sample is unbiased. It would be desirable to repeat this speed determination for a larger sample, selected purely on WAT morphology and with homogeneous jet sidedness measurements.

If the characteristic jet speeds are in fact lower than those of FR IIs, it may indicate a lower bulk speed throughout the jet, but would seem more likely to be a result of a stronger interaction between the jet and its environment in the case of WAT jets which are not protected by lobes, leading to a brighter, slower shear layer at the boundary of the jet. We note that some FR II jets which appear to lie outside their lobes are similarly bright and two-sided (e.g. 3C 438, Hardcastle et al. 1997). If WAT jets are relativistic in general, then ballistic models for the jet wiggles seen in many sources, and for the bends seen in 0647+693, are untenable; instead, these must be evidence for interaction between the jet and features of the external environment (either due to thermal or ram pressure). This in turn requires that the jets be light compared to the external medium, since the external sound speed is of the order of 1 per cent of the beaming speed (which, if it is due to a dissipative shear layer, may itself be an underestimate of the mean bulk speed of the flow).

Table 6. Straight jet flux densities and sidedness ratios

Source	Jet flux (mJy)	Counterjet flux (mJy)	Sidedness ratio
0647+693	0.60	0.13	4.79*
1231+674	2.26	1.84	1.23
1333+412	0.93	0.81	1.15
1433+553	1.17	0.33	3.55
2236–176	17.94	8.65	2.08
3C 465	22.46	4.21	5.34
1610–608	48.64	40.60	1.20

* Note that the straight jet region in this source is very short, so that the sidedness ratio may not be meaningful.

4.3 Jet termination

Our observations allow us to give a qualitative answer to the question posed in Section 1; how do the jets terminate? In fact, the larger sample gives results consistent with those already seen in 3C 130: jets in WATs terminate in a variety of ways, and do not necessarily show a compact ‘hotspot’. There are compact (comparable in size to the jet width), relatively bright features associated with the jet termination in 0647+693 (N jet), 1231+674 (N jet), 1333+412 (both jets) and 1433+553 (possibly both jets) but not clearly in 2236–176, 3C 465 or 1610–608, in which the jets simply make a smooth transition into the base of the plumes. Hotspots, where present, are not typically at the base of the plume, but some distance in, suggesting that the jet continues to be well collimated for some time after it enters the plume. Several sources, of which 1231+674 S is the best example, have jets that apparently penetrate undisrupted into the plumes for some distance before disappearing. This behaviour, also seen in 3C 130 S (Hardcastle 1998) seems to rule out models in which the jet disruption is related to an externally produced shock, or to the propagation of the jet across some other structure in the ICM; in such models the jet termination position would be fixed, so that there would be no reason for the plume to extend closer to the core than the end of the jet.

All the observations are, however, consistent with the idea (Hardcastle 1999) that the jets are ‘flapping’ in the bases of the plumes and show compact jet termination features only when they happen to impinge on the plume’s edge. The northern ‘hotspot’ of 0647+693 is particularly suggestive in this respect, as it lies on the outer edge of the plume. In this picture, the jet terminates where it does *now* because it enters the plume base and encounters the plume edge. If the structure of WATs is due to the properties of the ICM, then these must determine not the current jet termination point (which is ephemeral in any case) but the location of the base of the plume.

5 JET TERMINATION AND CLUSTER PROPERTIES

We were struck in carrying out this analysis by the wide range in the (projected) lengths of the inner jets that our target sources exhibit. If their cluster environments are responsible for the unique structure of WATs, then radio source properties such as jet length or distance to the plume base should be related to cluster richness, which we can parametrize in terms of the overall ‘cluster temperature’ determined from low-resolution X-ray observations. We emphasise that we are simply trying

to parametrize cluster richness by using this quantity; in general clusters will have temperature gradients and the central regions of the cluster may well be cooler than the value we quote. The advantage of working with a sample of Abell clusters is that X-ray observations already exist for many of our sources. Accordingly, we collated cluster temperatures from the literature for our targets; X-ray measurements were available for all but one (1231+674). To supplement our small sample, we also investigated the other sources from the Sakelliou & Merrifield (2000) sample that would have met our morphological selection criteria, listing those for which temperature measurements were available, and we also include the well-known WAT sources 3C 130 (Hardcastle 1998), Hydra A (Taylor et al. 1990), 4C34.16 (Sakelliou, Merrifield & McHardy 1996), Abell 2029 (Taylor, Barton & Ge 1994) and Abell 160 (Jetha et al. in prep.). We define the jet termination length as the mean of the two linear distances between the core and the compact ‘hotspot’ in the base of the plume, or the brightest feature in the base of the plume if no compact feature exists. The temperatures and termination lengths of the objects in the combined ‘sample’ (which is in no sense complete, but should not be biased in any obvious way) are listed in Table 7.

Cluster temperature is plotted as a function of jet termination length in Fig. 14. There is a clear trend in this plot, in the sense that hotter clusters have systematically shorter jets. The inverse correlation is significant at the 99 per cent confidence level on a two-tailed Spearman rank test. Although there is significant scatter in the correlation – unsurprisingly, given that all the distances should be corrected for an unknown projection factor and that the errors, not plotted for clarity, on the X-ray temperatures are sometimes large – its significance leads us to believe that we are seeing a real physical effect. Although it has been suggested that WATs are rare in ‘cooling flow’ clusters, two of the sample in Table 7 (Hydra A and A2029) would traditionally have fallen into this category¹. We find it interesting that the WATs in these clusters, though both small, seem to lie close to the relation established for non-‘cooling flow’ systems.

We consider the consequences of the length-temperature correlation for two WAT formation models.

(1) *Jet disruption at an interstellar medium/ICM interface* (Sakelliou & Merrifield 1999). In this model, the plumes are generated when the jet crosses the ISM/ICM interface. The steep density change in their environment possibly encourages the growth of large-scale instabilities in the shear layer of the jet; as our observations show, in some cases the jet does not disrupt at the base of the plume, but appears to carry on inside the plume. Detailed analysis of the properties of the environment of the jets and plumes will be able to shed more light on this issue. If the above is true, the observed distance between the core and the plume base gives a measurement of the size of the galactic atmosphere. The correlation shown in Fig. 14 would imply that the ISM of the central cluster galaxy is smaller in richer clusters. At first sight, this result seems to contradict common notions about the hot ISM in elliptical galaxies. Intuitively, one might expect the cores of richer clusters to be occupied by larger

¹ A2029 has been shown by Lewis, Stocke & Buote (2002) to have no spectral evidence for cooling X-ray emitting gas, and by Baker et al. (2003) to have no H α recombination emission, and so is unlikely to have a high deposition rate of cold matter.

Table 7. WAT jet termination lengths and cluster temperatures for the sample and for WAT sources from the literature

Radio name	Abell cluster	z	Jet termination length (kpc)	Reference for radio	Cluster temp (keV)	Reference for kT
0647+693	562	0.11	81	1	1.7	2
1231+674	1559	0.1049	35	1	—	
1333+412	1763	0.2278	20	1	6.9	3
1433+674	1940	0.1402	49	1	1.6	2
2236–176	2462	0.0742	44	1	1.5	2
3C 465	2634	0.0302	28	1	3.5	4
1610–608	3627	0.0157	13	1	7	5
3C 130	—	0.109	58	6	2.9	6
Hydra A	—	0.052	11	7	4.0	8
4C34.16	—	0.078	51	9	3.2	9
0110+152	160	0.0445	42	9	2.2	9
3C 40	194	0.018	59	10	2.6	11
1159+583	1446	0.104	19	12	2.6	2
1508+059	2029	0.076	3	12	7.8	3
1636+379	2214	0.1610	35	13	2.3	2

The horizontal line divides sources imaged in this paper from sources whose properties are taken from the literature. References are (1) This paper (2) Gómez et al. 1997 (3) David et al. 1993 (4) Schindler & Prieto 1997 (5) Tamura et al. 1998 (6) Hardcastle 1998 (7) Taylor et al. 1990 (8) David et al. 1990 (9) Unpublished *Chandra*, *XMM* and VLA data (10) O’Dea & Owen 1985 (11) Fukazawa et al. 1998 (12) Taylor et al. 1994 (13) O’Donoghue et al. 1990

galaxies (as a result of higher galaxy merging rate) and so would think that they should have larger ISMs. Earlier studies have indeed found positive correlations between the optical luminosity and temperature (and X-ray luminosity) for elliptical galaxies (e.g. Edge & Stewart 1991). However, these studies have largely been restricted to either isolated elliptical galaxies (or galaxies in poor environments), or X-ray faint galaxies, whose X-ray emission should be dominated by the stellar population. It is not clear that one should assume that the ISM in BCGs should also follow the stellar distribution. A plausible argument is that the correlation in Fig. 14 is caused by the higher pressures in the centres of rich clusters, which would naturally cause a hot ISM of a given mass to have a smaller radius. Another possibility is that the higher ram pressure from large-scale bulk motions in richer clusters is more efficient at stripping the ISM from the central cluster galaxy. We therefore cannot rule out the idea that the jet disrupts at the ISM/ICM interface, based on this correlation, although it does not give us any new information on *why* the jet should disrupt at this location. However, we would then expect a relationship between the temperature and the interface radius to hold in all BCGs, not just WAT hosts, which is a testable prediction of the model.

(2) *WATs as failed FRIs*. In the ‘cocoon-crushing’ model proposed by Hardcastle (1999), WATs are formed when the lobes of FRIs are driven out to large radii by buoyant forces as the internal lobe pressure drops, exposing the jet to the external medium. This would happen only for weak FRIs, in which the expansion speed, driven by the internal lobe pressure, became subsonic (i.e. the internal and external pressures became comparable) while the source was still close to the cluster centre. The speed at which buoyant forces can move radio-emitting plasma is determined by the external sound speed and the central density gradient: under free acceleration, the time taken to move a component of the source a given distance would be inversely proportional to temperature, with a relation of the form

$$t \propto \left(\frac{kT \nabla \rho}{\rho} \right)^{-1/2}$$

Both the external pressure and the sound speed are higher in rich, hot clusters, and so for a given jet power and a fixed density profile we would expect this process to take place earlier in the parent FRI’s life, making the resulting WAT shorter. Qualitatively, therefore, the observation that the plume bases are closer to the nucleus in hotter clusters is consistent with the failed-FRI model, although it does require that the jet luminosities of all the sources should be broadly similar. We note that this model would also predict stronger buoyant forces, and therefore a shorter core-plume base distance, in sources where the central density gradient was particularly high: this might explain why Hydra A, which lies in a well-known ‘cooling flow’ cluster, has a very short core-plume base distance even though the cluster temperature is not very high (Table 7).

6 CONCLUSIONS

We have detected well-collimated, bright inner jets in all of our small sample of WATs. The termination of these inner jets is often, but not universally, associated with a compact, hotspot-like radio feature. By analogy with the similar features in FRI radio galaxies, we may associate these compact features with shocks at which the jet interacts with some stationary medium. The fact that some sources *do not* show such termination features, but instead have jets that propagate undisturbed for some distance into the plumes, strongly suggests that the *current* location of the jet termination is not associated with some feature of the external medium, such as propagation across a shock front (Norman et al. 1988) or the ISM/ICM interface (Loken et al. 1995). Instead, it seems likely that the jet terminates where it does as a result of interaction with small-scale bulk motions of the plasma in the cluster and inside the plume base, which causes the end of the jet to move around inside the plume. Jet termination shocks are plausibly observed only when the jet happens to intersect with the edge of the plume. Jets which do not undergo jet termination shocks presumably merge into the larger-scale plume flow in a smoother way.

However, the location of the plume base appears to be a function of the temperature of the host cluster, providing for the first time some direct evidence that the structure of WATs is determined by their cluster environments. The model in which the jet-plume transition of WATs is related to the ISM/ICM interface (which does have the attractive feature that it ‘predicts’ a scale length for the transition of tens of kpc, as observed) can account for this only if the ISM/ICM interface radius is smaller for hotter clusters. We are not aware of observations that test this prediction at this time, but in a future paper we will return to this question, and to the general problem of the physical conditions around the jets and jet terminations, using our detailed *Chandra* and *XMM-Newton* observations of WAT cluster environments. Radio observations of a much larger sample of WATs with similar resolution and sensitivity would also be valuable to test the generality of our conclusions.

ACKNOWLEDGEMENTS

The National Radio Astronomy Observatory is a facility of the National Science Foundation operated under cooperative agreement by Associated Universities, Inc. The Australia Telescope is funded by the Commonwealth of Australia for operation as a National Facility managed by CSIRO. We are grateful to Jean Eilek and Debora Katz-Stone for allowing us to use their archival VLA data, to the staff of the ATNF, particularly Tasso Tzioumis, for their help in carrying out the ATCA observations and in organizing our observing visits, and to Nazirah Jetha for discussion of WAT properties. In collating X-ray data for the clusters we made use of the BAX (Base de données Amas de galaxies X) system at <http://webast.ast.obs-mip.fr/bax/>. We thank an anonymous referee for comments that helped us to improve the paper.

MJH thanks the Royal Society for a Research Fellowship. MJH and IS would like to thank the Universities of Birmingham and Bristol, respectively, for hospitality during the preparation of this paper. IS is grateful to the Mullard Space Science Laboratory for funding during the early stages of this work.

APPENDIX A: THE JETS OF 3C 75

The well-known twin source 3C 75 (Owen et al. 1985), at a redshift of 0.0240, is often classed as a wide-angle tail on the basis of its large-scale structure (e.g. O’Donoghue et al. 1993). It is certainly the case that the object lies at the centre of a cluster, Abell 400, and that its large-scale plumes bend in a manner similar to those of some of the WATs in our sample, although the radio luminosities of the two sources are a factor ~ 5 lower than the typical luminosity of our WATs, and much more comparable to those of normal twin-jet FRIs. However, we have excluded it from consideration here on the basis that its inner jets have a large opening angle and that it does not show an abrupt jet-plume transition with a bright plume base; we would instead describe it as a pair of normal twin-jet FRI sources in a rich environment. To justify this, we present here a previously unpublished high-resolution VLA image of the inner parts of the source. The source was observed by one of us (MJH) at two frequencies, 8.415 and 8.465 GHz, with a 50-MHz bandwidth for 2 hours in B-configuration on 1995 Nov 28 and 1 hour in

C-configuration on 1994 Nov 10. The data were reduced as described in Section 2. Fig. A1 shows the resulting image. It is clear that the jets of 3C 75 are well resolved, with an opening angle much larger than those of the WATs in our sample (compare 3C 465, at a similar redshift) and have no strong side-to-side asymmetry, as is typical for normal FRI jets at more than a few kpc from the core. The N jet also displays the transition between parallel and perpendicular magnetic field characteristic of normal FRI jets, which takes place at a distance from the core about 8 arcsec (4 kpc). The fainter S jets have a perpendicular magnetic field from about 16 arcsec (8 kpc). There is no bright flare point or abrupt change in opening angle in these images, or in the lower-resolution but more sensitive images of Owen et al. (1985) or Eilek & Owen (2002); instead, the jets merge seamlessly into the plumes. We thus feel justified in excluding this object from our sample of WATs, although it is present in the parent sample of bent sources (Sakelliou & Merrifield 2000).

REFERENCES

- Baker, K., Bremer, M.N., Jaffe, W., Hardcastle, M.J., 2003, MNRAS submitted
- Blandford, R.D., Icke, V., 1978, MNRAS, 185, 527
- Böhringer, H., Neumann, D.M., Schindler, S., Kraan-Korteweg, R.C., 1996, ApJ, 467, 168
- Christiansen, W.N., Frater, R.H., Watkinson, A., O’Sullivan, J.D., Lockhart, I.A., Goss, W.M., 1977, MNRAS, 181, 183
- David, L.P., Arnaud, K.A., Forman, W., Jones, C., 1990, ApJ, 356, 32
- David, L.P., Slyz, A., Jones, C., Forman, W., Vrtillek, S.D., 1993, ApJ, 412, 479
- Edge, A.C., Stewart, G.C., 1991, MNRAS, 252, 428
- Eilek, J.A., Owen, F.N., 2002, ApJ, 567, 202
- Eilek, J.A., Burns, J.O., O’Dea, C.P., Owen, F.N., 1984, ApJ, 278, 37
- Fukazawa, Y., Makishima, K., Tamura, T., Ezawa, H., Xu, H., Ikebe, Y., Kikuchi, K., Ohashi, T., 1998, PASJ, 50, 187
- Gómez, P.L., Pinkney, J., Burns, J.O., Wang, Q., Owen, F.N., Voges, W., 1997, ApJ, 474, 580
- Hardcastle, M.J., 1998, MNRAS, 298, 569
- Hardcastle, M.J., 1999, A&A, 349, 381
- Hardcastle, M.J., Alexander, P., Pooley, G.G., Riley, J.M., 1997, MNRAS, 288, 859
- Hardcastle, M.J., Alexander, P., Pooley, G.G., Riley, J.M., 1998, MNRAS, 296, 445
- Hardcastle, M.J., Alexander, P., Pooley, G.G., Riley, J.M., 1999, MNRAS, 304, 135
- Jones, P.A., McAdam, W.B., 1992, ApJS, 80, 137
- Jones, P.A., McAdam, W.B., 1996, MNRAS, 282, 137
- Katz-Stone, D.M., Rudnick, L., Butenhoff, C., O’Donoghue, A.A., 1999, ApJ, 516, 716
- Kraan-Korteweg, R.C., Woudt, P.A., Cayatte, V., Fairall, P., Balkowski, C., Henning, P.A., 1996, Nat, 379, 519
- Leahy, J.P., 1984, MNRAS, 208, 323
- Leahy, J.P., 1993, in Röser H.-J., Meisenheimer K., eds, Jets in Extragalactic Radio Sources, Springer-Verlag, Heidelberg, p. 1
- Ledlow, M.J., Owen, F.N., 1995, AJ, 109, 853
- Lewis, A.D., Stocke, J.T., Buote, D.A., 2002, ApJ, 573, L13
- Loken, C., Roettiger, K., Burns, J.O., 1995, ApJ, 445, 80
- Norman, M.L., Burns, J.O., Sulkanen, M.E., 1988, Nat, 335, 146
- O’Dea, C.P., Owen, F.N., 1985, AJ, 90, 927
- O’Donoghue, A.A., Owen, F.N., Eilek, J.A., 1990, ApJS, 72, 75
- O’Donoghue, A.A., Eilek, J., Owen, F., 1993, ApJ, 408, 428
- Owen, F.N., Ledlow, M.J., 1997, ApJS, 108, 41
- Owen, F.N., Ledlow, M.J., Keel, W.C., 1995, AJ, 109, 14
- Owen, F.N., O’Dea, C.P., Inoue, M., Eilek, J.A., 1985, ApJ, 294, L85
- Sakelliou, I., Merrifield, M.R., 1999, MNRAS, 305, 417

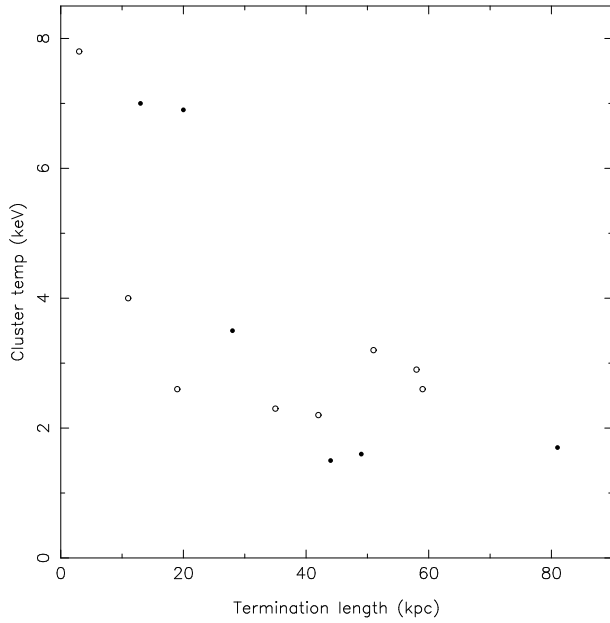


Figure 14. Cluster temperature (kT , keV) against jet termination length L (kpc), as defined in the text, for the WAT host clusters listed in Table 7. Filled circles denote sources in our own sample, while open circles denote sources taken from the literature.

- Sakelliou, I., Merrifield, M.R., 2000, MNRAS, 311, 649
 Sakelliou, I., Merrifield, M.R., McHardy, I.M., 1996, MNRAS, 283, 673
 Schindler, S., Prieto, M.A., 1997, A&A, 327, 37
 Stickel, M., Kühn, H., 1994, A&AS, 103, 349
 Struble, M.F., Rood, H.J., 1999, ApJS, 125, 35
 Tamura, T., Fukazawa, Y., Kneda, H., Makishima, K., Tashiro, M.,
 Tanaka, Y., Böhringer, H., 1998, PASJ, 50, 195
 Taylor, G.B., Barton, E.J., Ge, J., 1994, AJ, 107, 1942
 Taylor, G.B., Perley, R.A., Inoue, M., Kato, T., Tabara, H., Aizu, K.,
 1990, ApJ, 360, 41
 Wardle, J.F.C., Aaron, S.E., 1997, MNRAS, 286, 425

This paper has been typeset from a $\text{\TeX}/\text{\LaTeX}$ file prepared by the author.

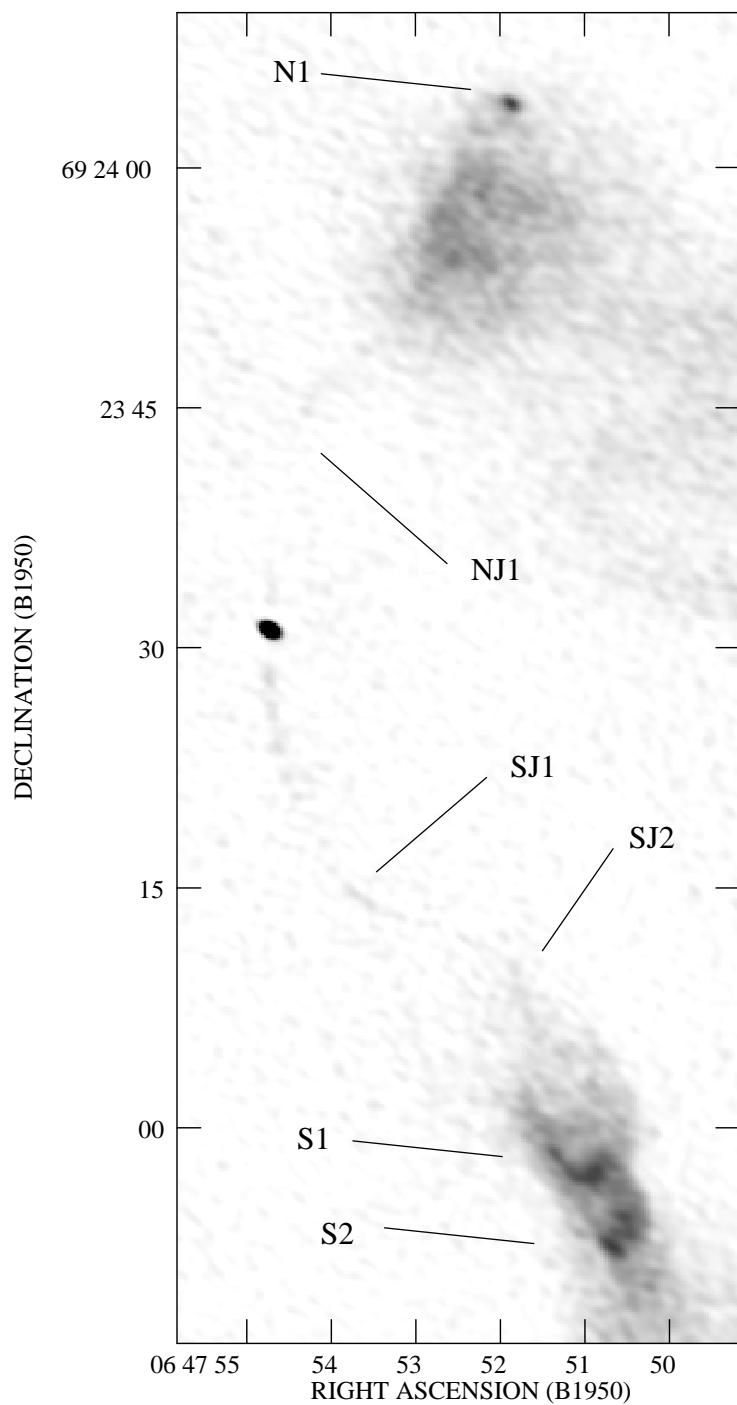


Figure 2. 0.9×0.6 -arcsec resolution map of 0647+693. Black is 1 mJy beam^{-1} .

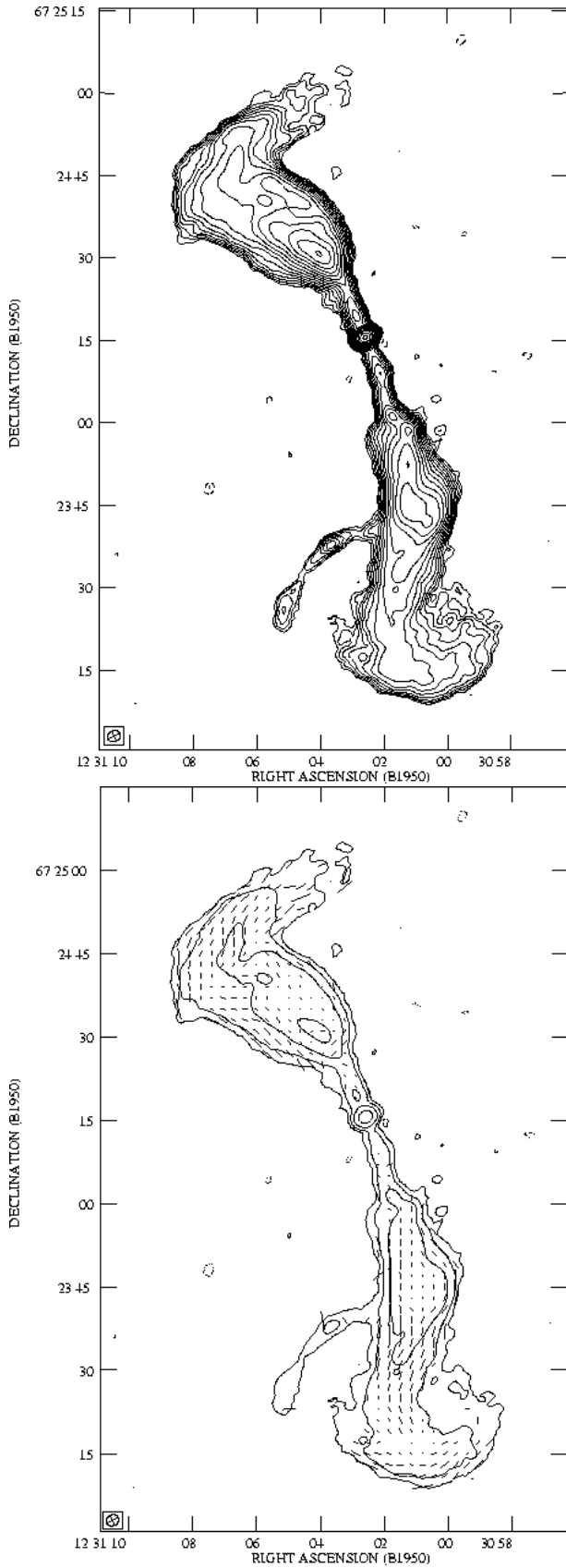


Figure 3. 2-arcsec resolution map of 1231+674. As Fig. 1, but lowest contour level is $40 \mu\text{Jy beam}^{-1}$.

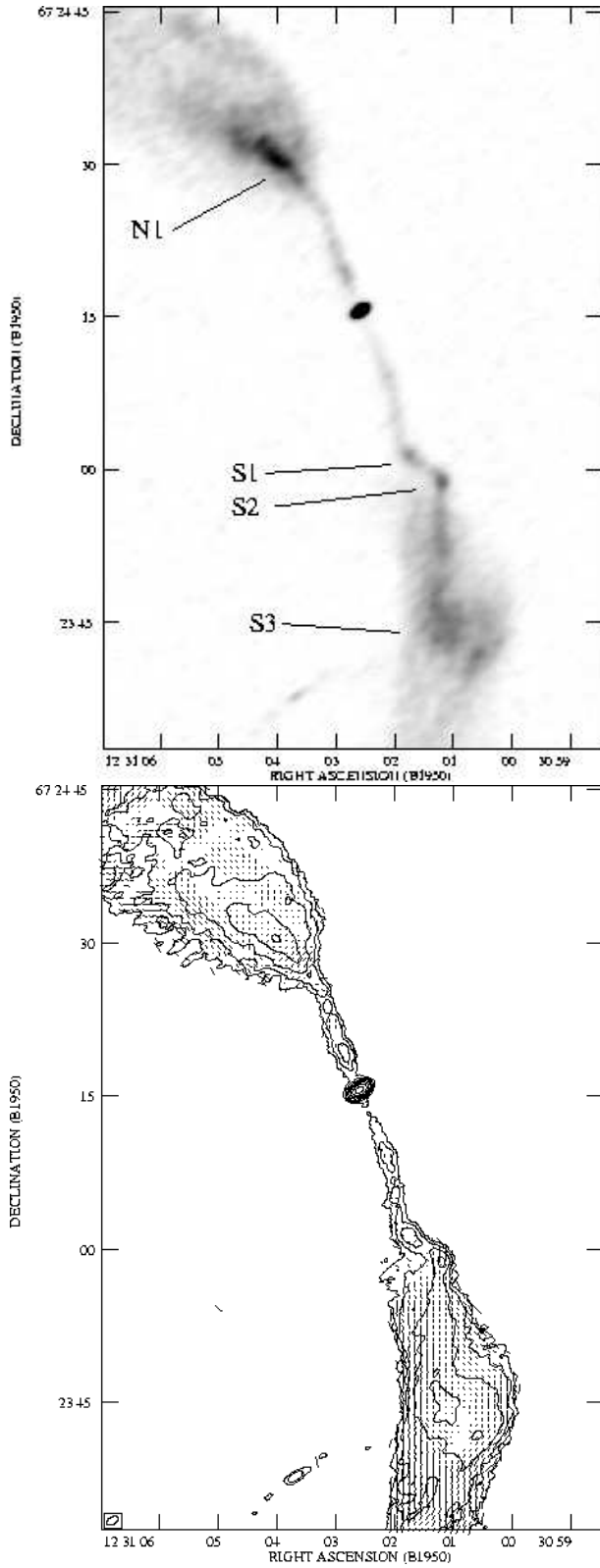


Figure 4. 1.24×0.73 -arcsec resolution map of 1231+674. Left: black is 1 mJy beam^{-1} . Right: As Fig. 1 (right), but lowest contour level is $60 \mu\text{Jy beam}^{-1}$.

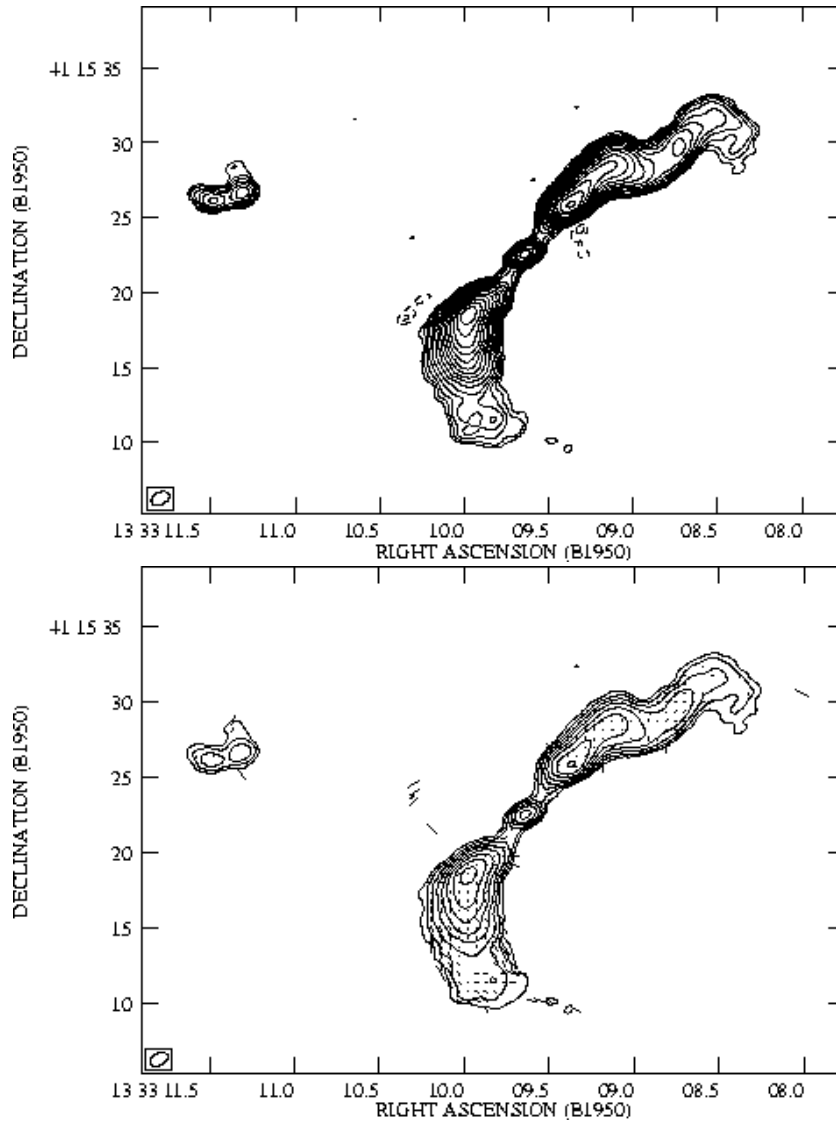


Figure 5. 1.3×0.8 -arcsec resolution map of 1333+412. As Fig. 1, but lowest contour level is $80 \mu\text{Jy beam}^{-1}$.

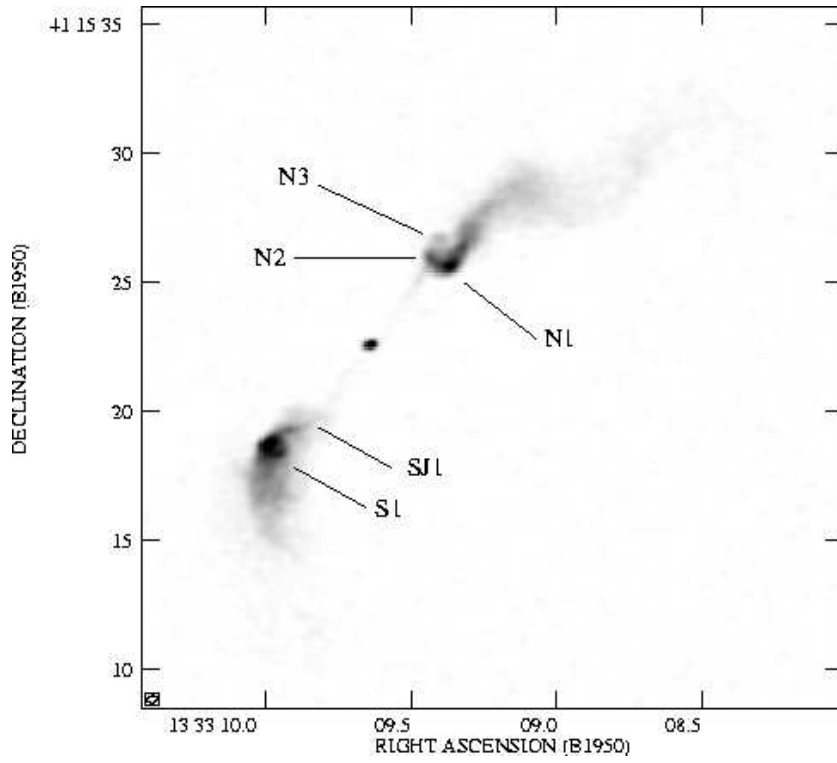


Figure 6. 0.38×0.27 -arcsec resolution map of 1333+412. Black is 2 mJy beam^{-1} .

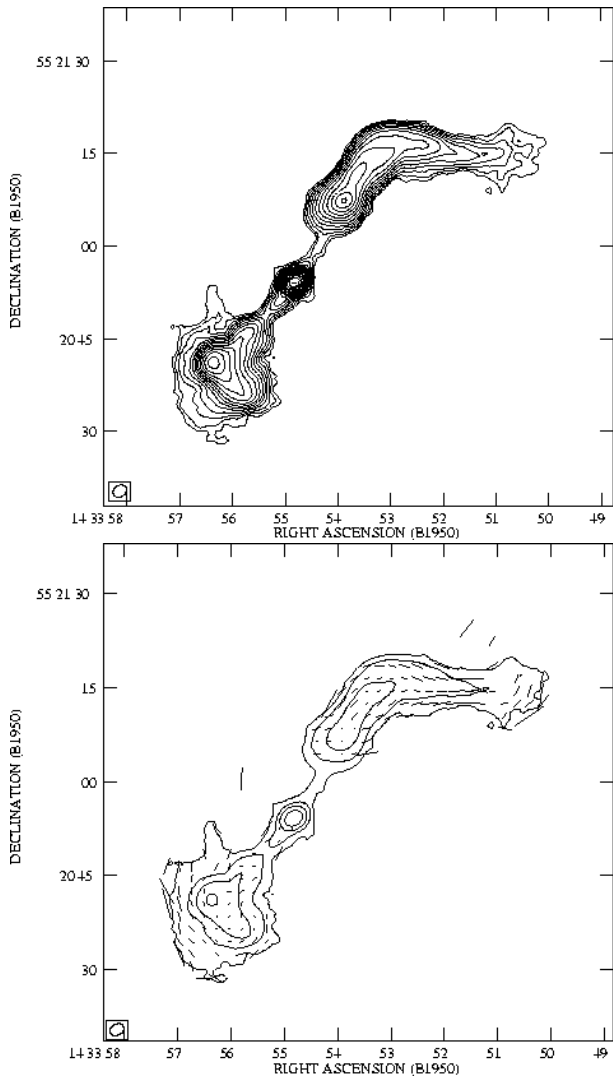


Figure 7. 2.2×1.8 -arcsec resolution map of 1433+553. As Fig. 1, but lowest contour level is $80 \mu\text{Jy beam}^{-1}$.

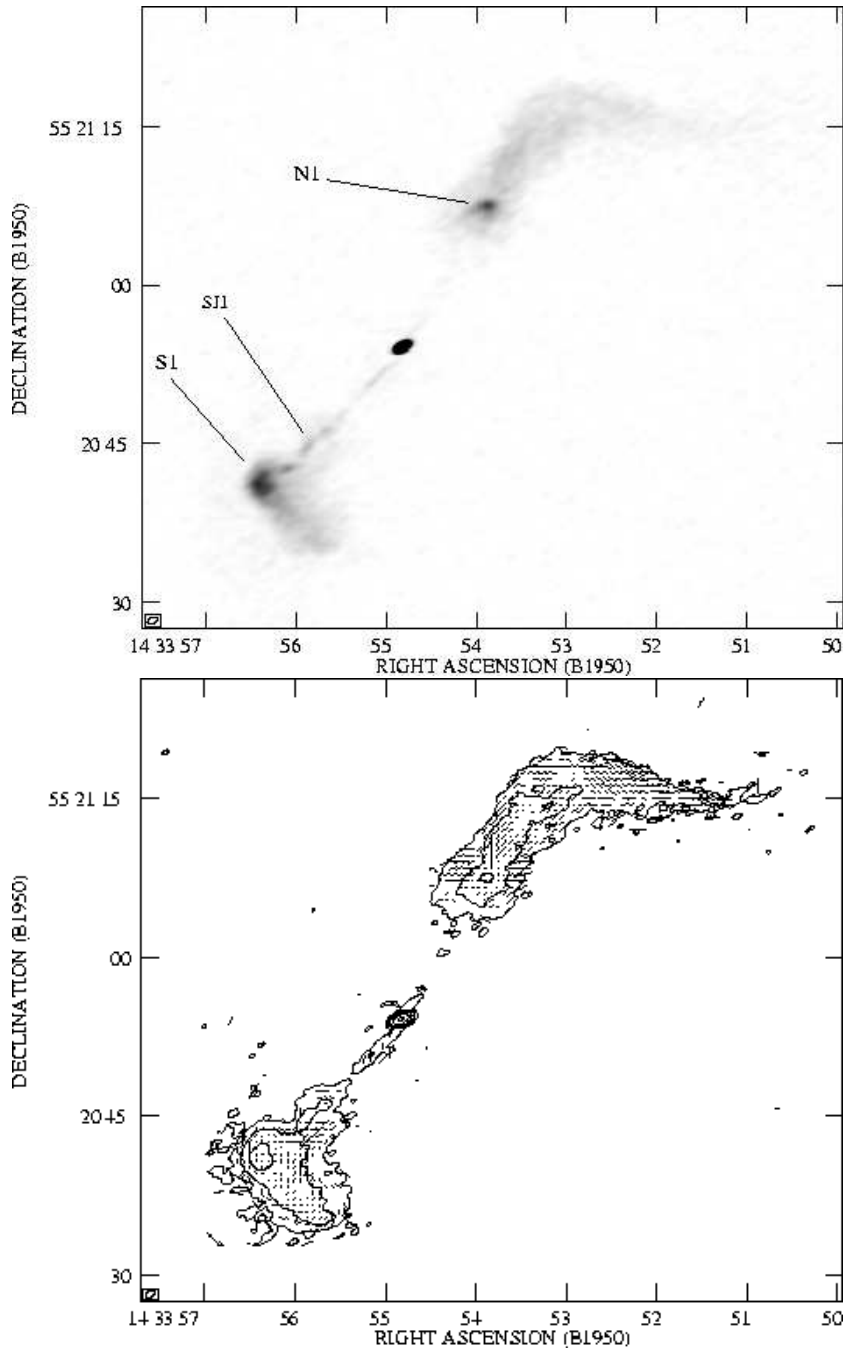


Figure 8. 1.0×0.55 -arcsec resolution maps of 1433+553. Top: black is $1.5 \text{ mJy beam}^{-1}$. Bottom: as Fig. 1, but lowest contour is $100 \mu\text{Jy beam}^{-1}$.

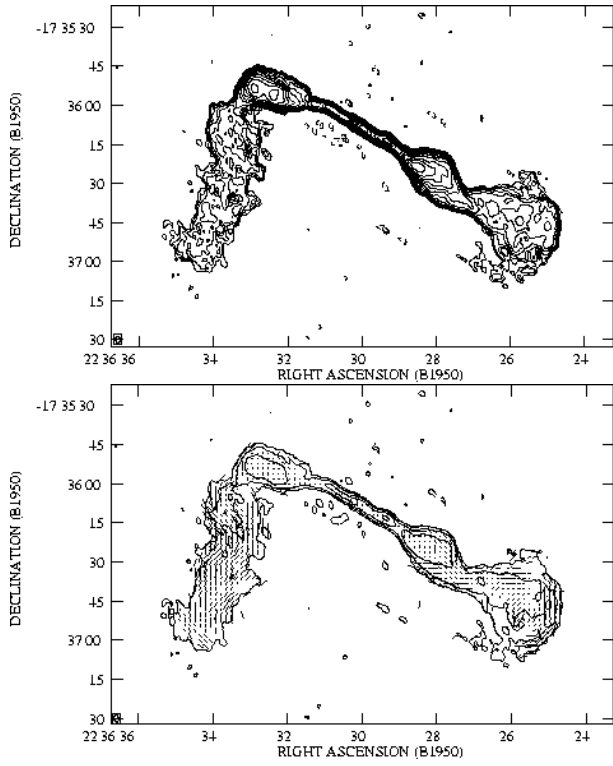


Figure 9. 2.6×1.8 -arcsec resolution map of 2236–176. As Fig. 1, but lowest contour level is $80 \mu\text{Jy beam}^{-1}$.

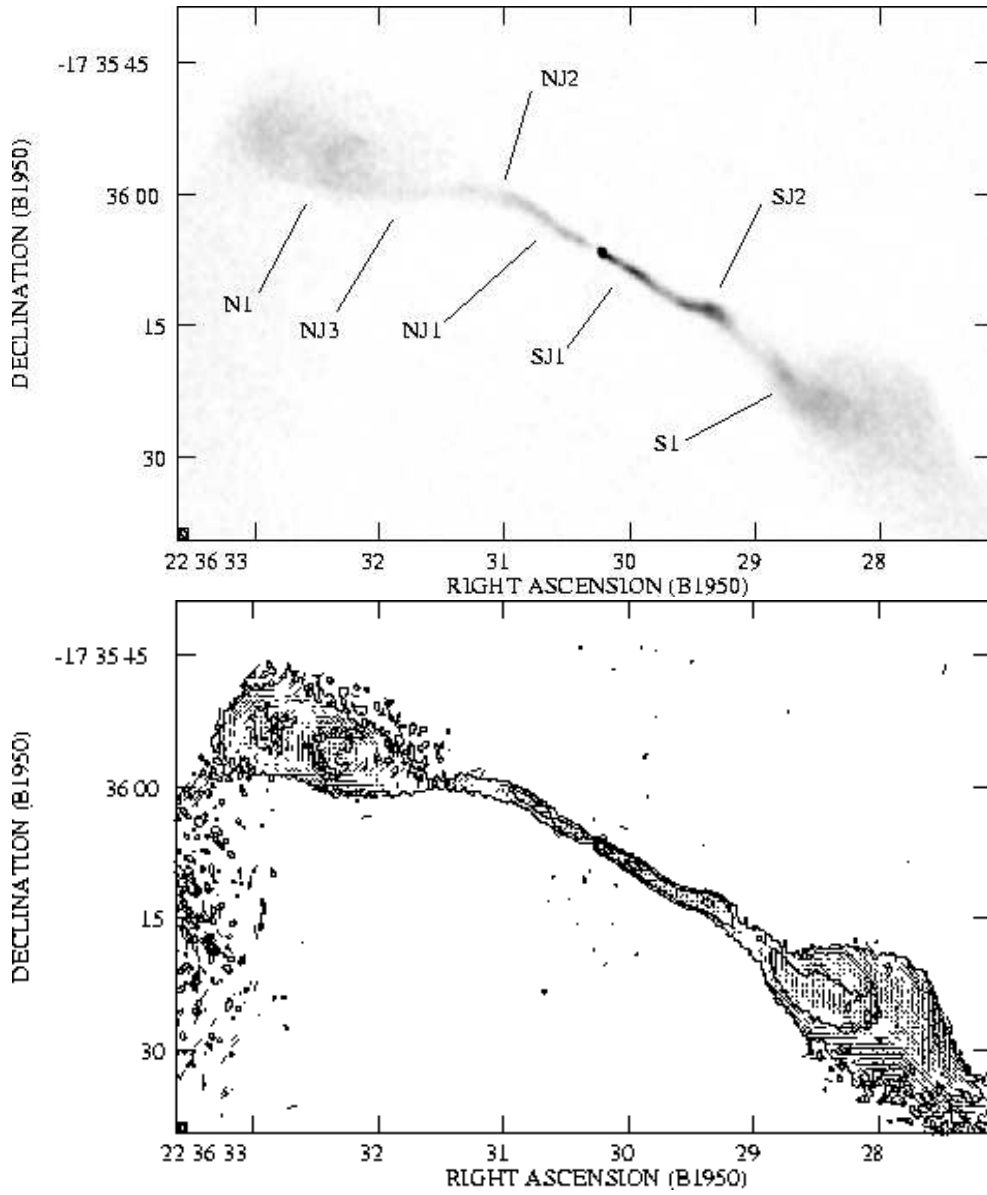


Figure 10. 0.78×0.52 -arcsec resolution map of 2236–176. Top: black is $1.5 \text{ mJy beam}^{-1}$. Bottom: As Fig. 1 (right), but lowest contour level is $60 \mu\text{Jy beam}^{-1}$.

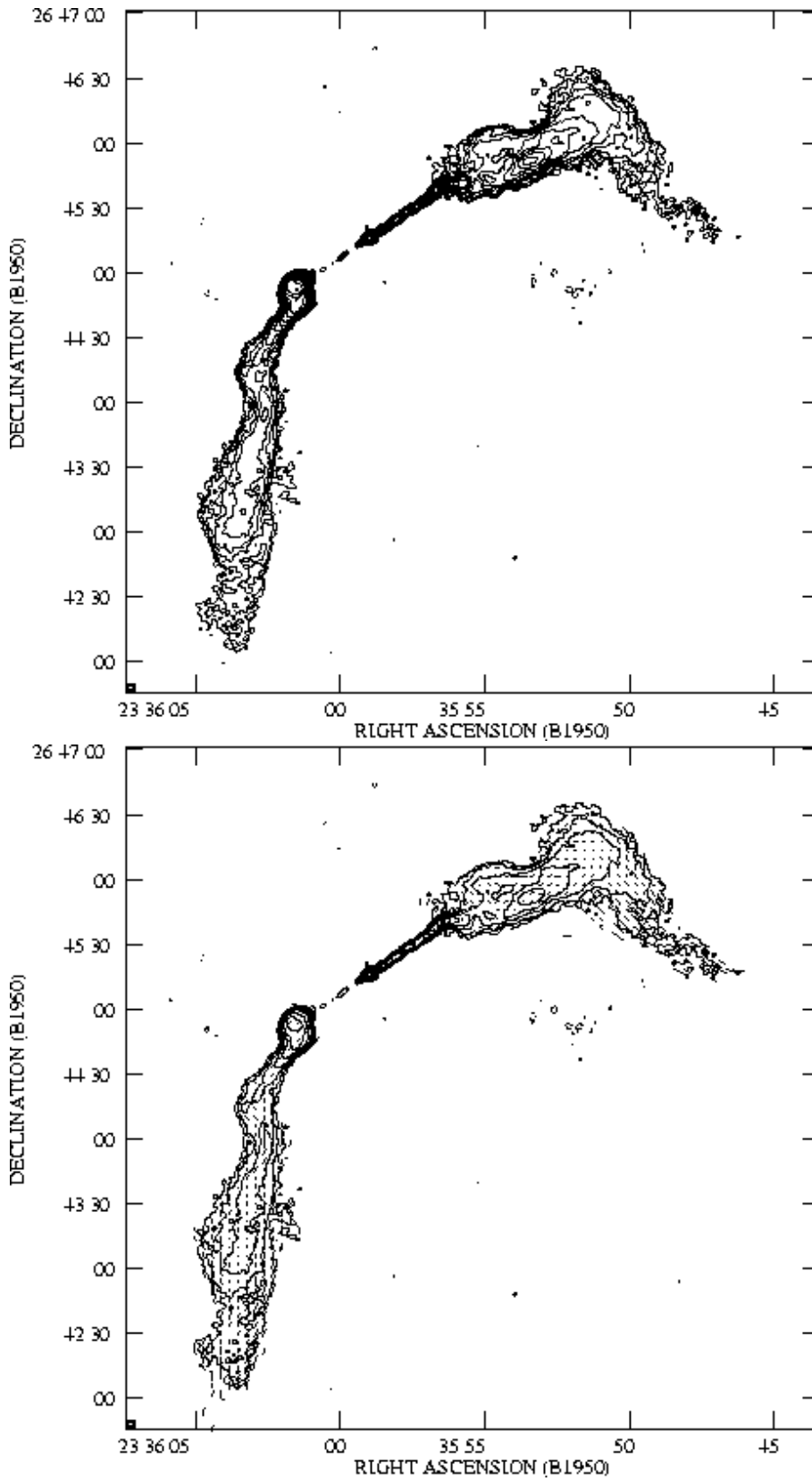


Figure 11. 2.6×2.0 -arcsec resolution map of 3C 465. As Fig. 1, but lowest contour level is $130 \mu\text{Jy beam}^{-1}$.

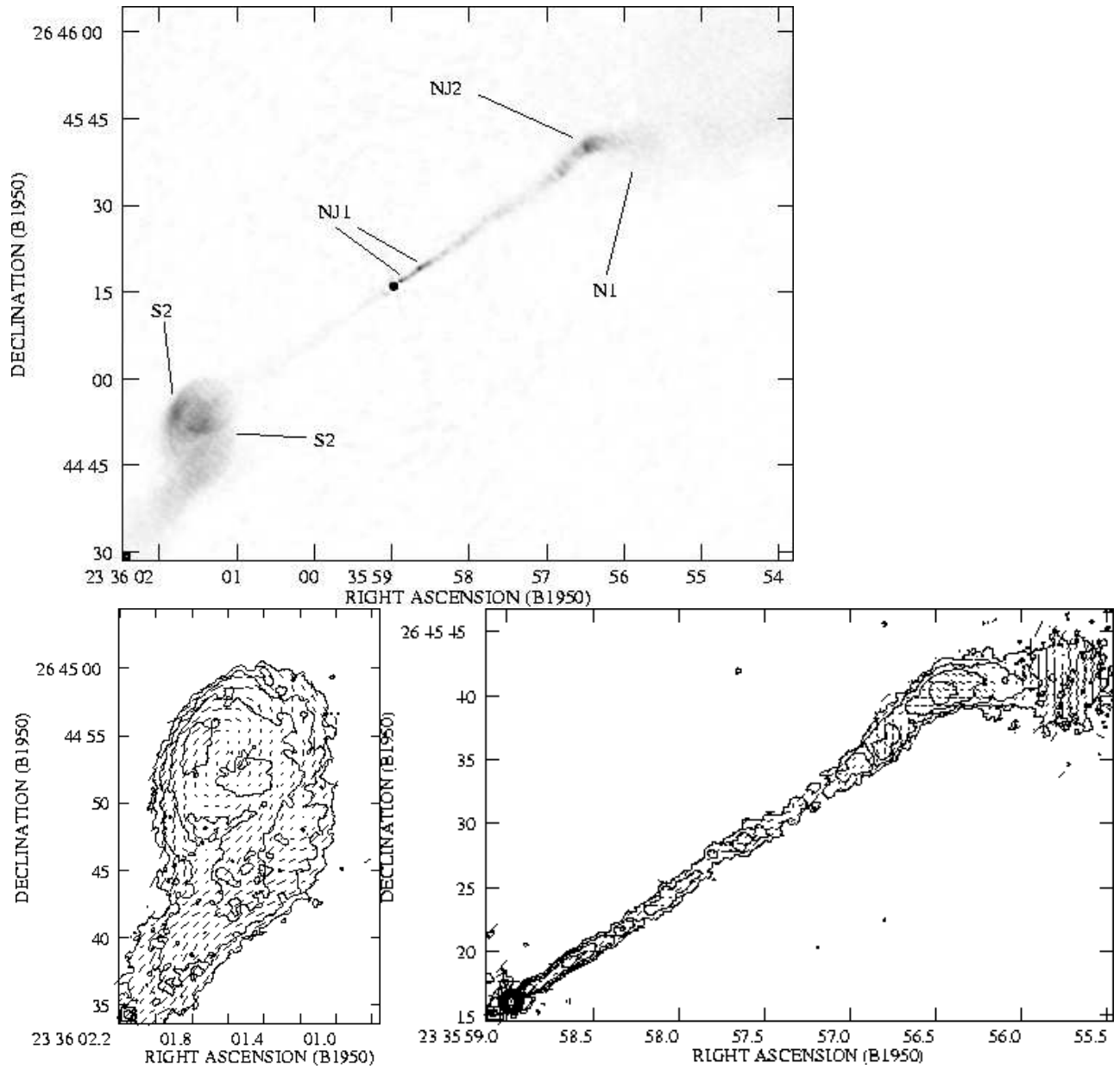


Figure 12. 0.61×0.60 -arcsec resolution maps of 3C 465. Top: black is 2 mJy beam^{-1} . Bottom: as Fig. 1, but lowest contour level is $100 \mu\text{Jy beam}^{-1}$. The two polarization maps show the structure in (left) the S plume base and (right) the jet.

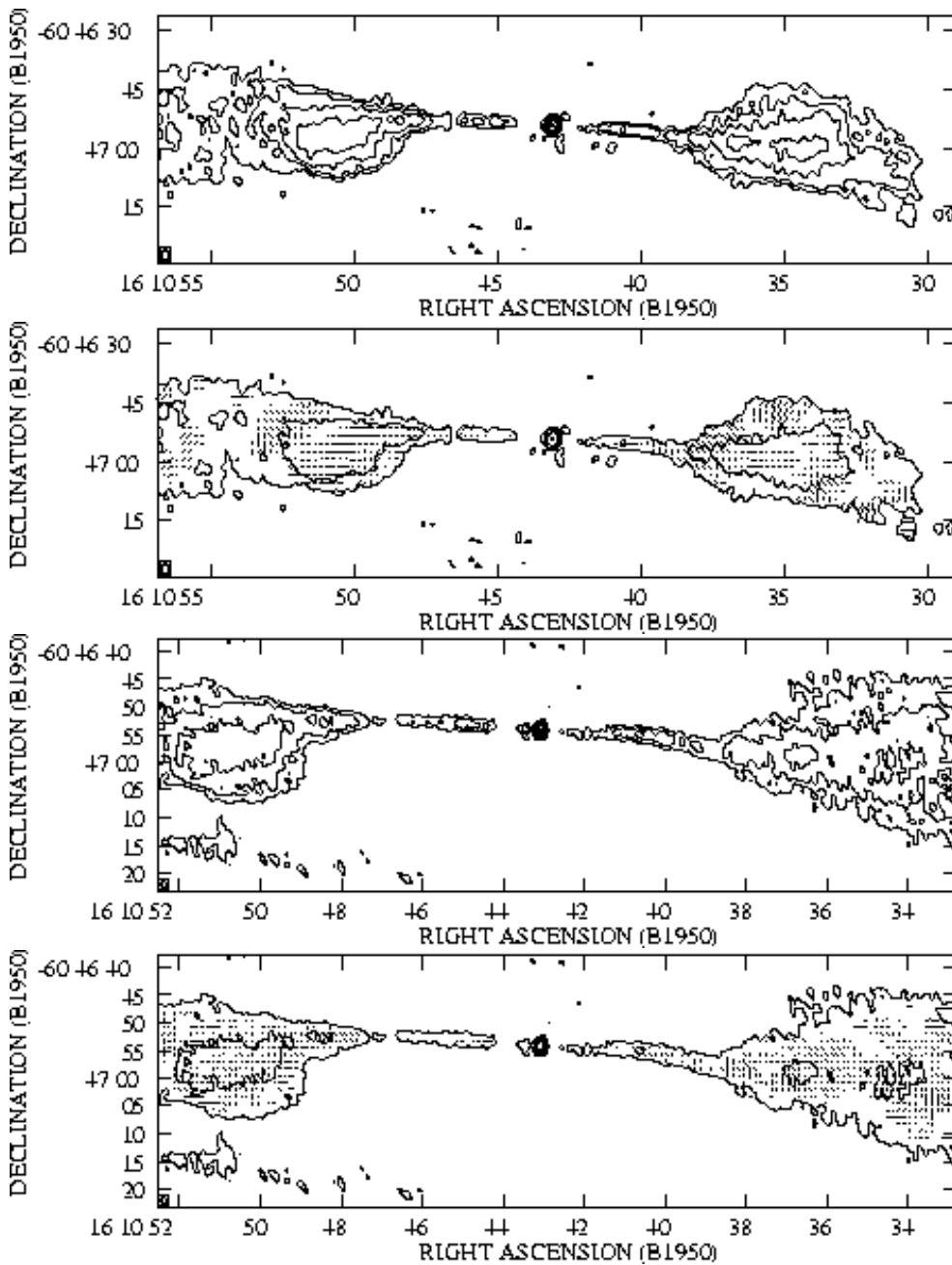


Figure 13. 5 and 8-GHz maps of 1610–608. Top: C-band maps at 2.5×1.8 arcsec resolution: lowest contour is 2 mJy beam^{-1} and contours increase logarithmically by a factor 2 (upper panel) and 4 (lower panel). Bottom: X-band maps at 1.3×1.0 arcsec resolution: lowest contour is $0.8 \text{ mJy beam}^{-1}$, contours as above.

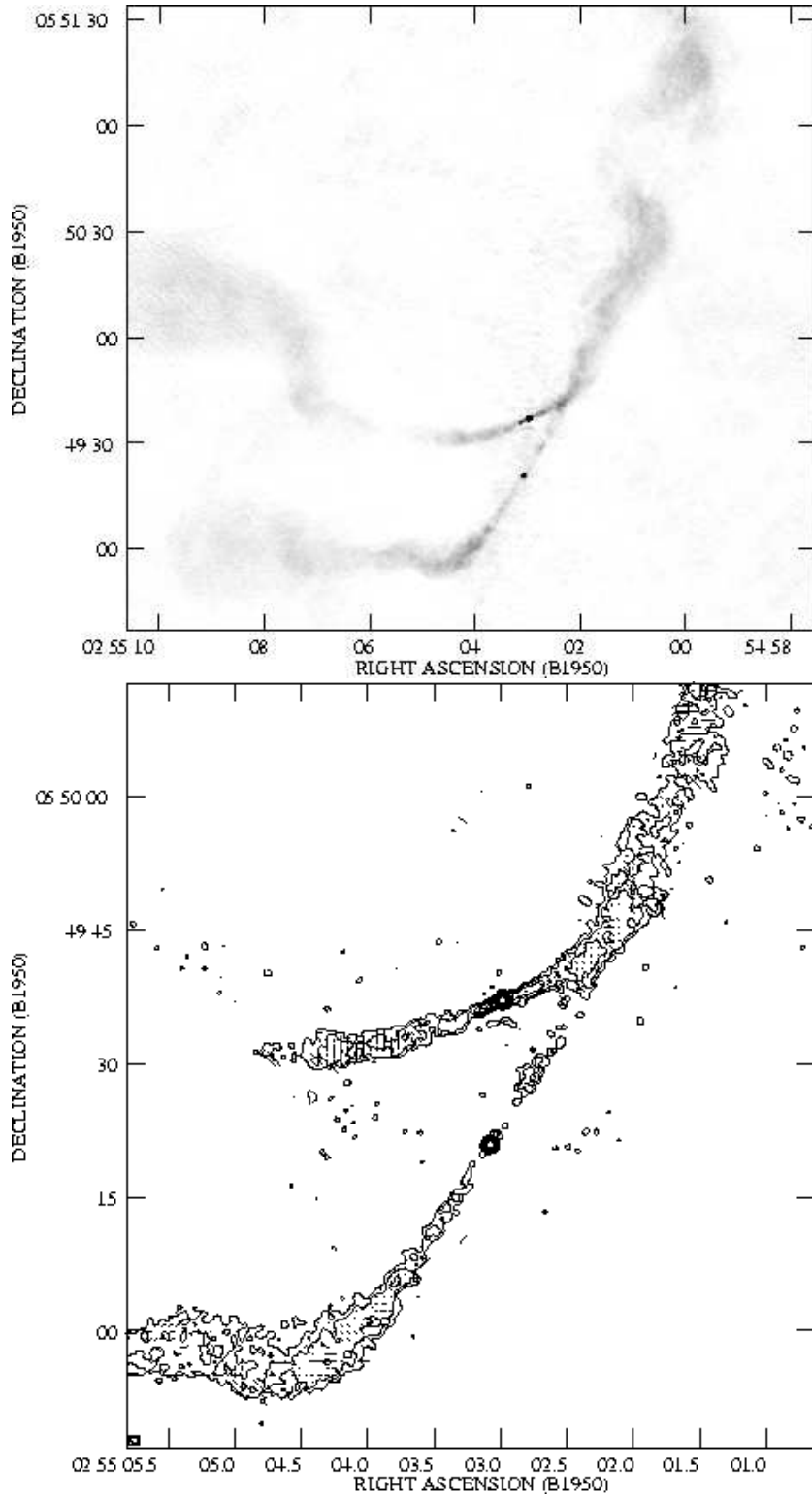


Figure A1. 0.77×0.73 -arcsec resolution map of the double twin-jet source 3C 75. Top: the jets and plumes. Black is 1 mJy beam^{-1} . Bottom: the inner jets. As Fig. 1, but lowest contour level is $90 \mu\text{Jy beam}^{-1}$. Contours increase by a factor 2.